lubricants

MDPI

Article

Tribological Properties and Lubrication Mechanism of Biomimetic Rectangular Micro/Nanogrid Structures of Mechanical Transmission Sliding Plates

Yunliang Wang [1], Kang Yang [2,3,*] and Jun Tang [4]

[1] School of Electromechanical Engineering, Zhengzhou Electric Power Technology College, Zhengzhou 451450, China; wangyunl2008@163.com
[2] School of Mechanical and Electrical Engineering, Linzhou College of Architectural Technology, Anyang 456550, China
[3] School of Mechanical and Aeronautical Manufacturing Engineering, Anyang Institute of Technology, Anyang 455000, China
[4] School of Material and Science, Central South University of Forestry and Technology, Changsha 410004, China
* Correspondence: angongyangkang@163.com; Tel./Fax: +86-372-2986271

Abstract

To optimize the tribological properties of a mechanical transmission skateboard, rectangular micro/nanogrid structures of different sizes are studied. The reciprocating sliding tests are carried out under friction and wear. The results show that with an increase in the lengths from 330 to 484 μm and widths from 247 to 363 μm of the grid structures, the friction coefficients and wear rates first decrease and then increase. This results in the smallest friction coefficient and wear rate of the TCSC-G-4 with 440 μm length and 330 μm width. This is because the micro/nanogrid structures provide the lubricant SnAgCu-CaF_2 (SC), which is sufficient for lubrication film formation. During wear, SnAgCu deformation and CaF_2 rolling lead to mixed lubrication that is dominated by the rolling, sliding and roller–sliding, enhancing the plastic flow of the lubrication film for surface repair. This is of great significance for guiding the bionic tribological designs of the skateboard.

Keywords: micro/nanogrid structures; bionics; sliding wear; lubrication mechanisms; tribological behavior

1. Introduction

During the sliding wear process, the stable tribological properties of mechanical transmission sliding plates directly affect their working stability [1]. This is one of the important factors restricting the good development of the manufacturing industry [2,3]. To address this issue, our team systematically reviews a large number of relevant reports on friction, wear and lubrication stability, and finds that these studies mainly focus on the important effects of self-lubricating materials [4,5], lubrication coatings [6–8] and surface structures on tribological properties [9], while an in-depth exploration of the lubrication stability is lacking.

Although the aforementioned studies have improved the lubrication performance of friction interfaces, the achieved lubrication stability still cannot meet the industrial need, which is specifically reflected in three aspects: First, the lubricants in the bulk self-lubricating materials are easily hindered by their matrix, making it difficult for the migration and enrichment of the lubricants on the wear scars, thus resulting in the poor regulation of wear stability of the self-lubricating materials [10–12]. Second, under the

Check for updates

Received: 3 August 2026
Revised: 24 August 2026
Accepted: 26 August 2026
Published: 10 September 2026

Copyright: © 2026 by the authors. Licensee MDPI, Basel, Switzerland. This article is an open access article distributed under the terms and conditions of the Creative Commons Attribution (CC BY) license.

dry sliding wear condition, the lubrication coatings are subject to the interaction of wear force and friction heat, which make them prone to microdamage, and the coatings may be peeled off from them matrix; this further produces a significant effect on lubrication stability [13,14]. Third, the micro-structure preparation on the wear scar promotes the migration and enrichment of solid lubricants, which improves lubrication behaviors, but this lubrication stability has not been given sufficient attention [15,16], leading to to the situation that the contact interface has good lubrication behavior, and the working stability cannot self-adapt to the developed needs of the manufacturing industry.

In accordance with relevant reports on bionic lubrication [17,18], we find that controlling surface micro-structure and lubricant selection is an effective method for improving lubrication behaviors. This ignores the effect of the micro-scale structure on tribological properties and lubrication stability. These tests confirm that excessively large microstructure sizes increase the lubricant filling and improve the friction-reducing behavior of the wear interface, but this weakens the bearing ability of the contact surface; it leads to a decrease in wear resistance, affects lubrication stability, and then restricts manufacturing development. To solve this problem for acquiring excellent tribological properties of mechanical transmission sliding plates, the intention of this study is to design rectangular microgrid structures by drawing on the micro/nano-structure of a butterfly wing and then control the grid scales. The SnAgCu-CaF_2 (SC) is well chosen, fills into the microgrid structures using laser sintering and infiltration technology, and then acquires the rectangular micro/nanogrid structure for lubrication. By exploring the effect of the lengths and widths of the micro/nanogrid structure on the tribological property, the micro/nanogrid structures are well selected for optimal lubrication; they can meet the good requirements of lubrication behavior and wear stability of the mechanical transmission sliding plates, contributing to manufacturing development.

From the foregoing discussions, the main innovation of this study is summarized as follows: First, a large amount of solid lubricants, SC, are stored in the rectangular micro/nanogrids, enabling sustained lubricant supply. Second, in contrast with those of the bulk self-lubricating composite, the SC in the surface microgrid has a short migration to the contact interface, thus ensuring self-responsive lubrication. Third, this work adopts bionic rectangular grids inspired by butterfly wings and establishes a good relationship between grid sizes and tribological behaviors.

The scientific contribution of this study is summarized as follows: First, the novel bionic lubrication systems are well constructed for the mechanical transmission sliding plates. Second, the influence of grid dimensions on the tribological behavior is revealed, and the optimal grid size is determined. Third, the synergistic lubrication of SnAgCu deformation, CaF_2 rolling and the rolling–sliding is clarified. This work provides good guidance for the bionic wear design of the mechanical transmission sliding plate.

2. Sample Preparation and Measurements

2.1. Sample Preparation

Swallowtail butterflies are widely adopted as the biological prototypes in tribology. Their wing scales are well observed, and the main longitude ridges and transverse ribs intersect orthogonally. This perpendicular division forms rectangular micro-units with a fixed ratio, effectively reduces the flight drag and mitigates the abrasion of the wing surface. To obtain good tribological properties in mechanical transmission plates, proportional rectangular micro/nanogrids on commercial TC surfaces are well designed by drawing on the micro/nano-structures of butterfly wings. Three tests ensure that the TC is mainly composed of 89.04 wt.%-Ti, 6.04 wt.%-Al, 4.23 wt.%-V, 0.31 wt.%-Fe, 0.21 wt.%-O, 0.10 wt.%-C, 0.05 wt.%-N, 0.02 wt.%-H. A 3D design model of the microgrid structure of the TC-G4

is shown in Figure 1a. Table 1 presents the main dimensions of the rectangular microgrid structures. It can be seen from Figure 1a and Table 1 that the designed depth D of the rectangular microgrid structure is 200 μm, the spacing S is 200 μm, and the ratio of length (L) to width (W) is approximately 1.33. The test results show that the errors between manufactured sizes and the designed dimensions are less than 3.5% and confirm that the rectangular grid structure has been successfully prepared in the TC-G4 surface. Among them, the scanning power of the CT-MF30 laser sintering equipment is 27 kW, scanning wavelength is 1064 nm, scanning speed is 400 mm/s, the scanning frequency is 30 kHz, the end delay is 200 μs, the corner delay is 100 μs, and switching delay is 300 μs.

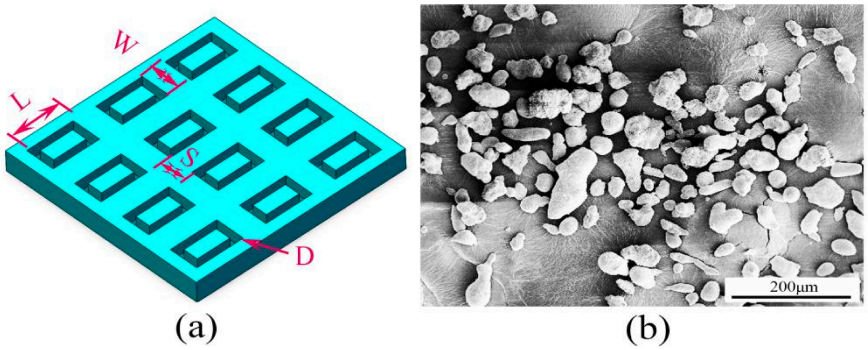


Figure 1. 3D model of the proportional rectangular grid microstructures of the TC-G-4 sample (**a**) and FESEM morphology of the mixed lubricant SC (**b**).

Table 1. Corresponding dimensions of the rectangular grids prepared for the TC surfaces.

Sample Names	Width W (μm)	Length L (μm)	Space S (μm)	Depth D (μm)	Distribution Proportion	Common Ratios	
						Length-Width Ratio ($L_{TC\text{-}G\text{-}n}$:$W_{TC\text{-}G\text{-}n}$)	Length or Width Ratios ($L_{TC\text{-}G\text{-}n}$ + 1:$L_{TC\text{-}G\text{-}n}$; $W_{TC\text{-}G\text{-}n}$ + 1:$W_{TC\text{-}G\text{-}n}$)
TC	0	0	0	0	0%	-	-
TC-G-1	248	330	200	200	25.8%	1.33	1.1
TC-G-2	272	363	200	200	27.9%	1.33	1.1
TC-G-3	300	400	200	200	30.0%	1.33	1.1
TC-G-4	330	440	200	200	32.1%	1.33	1.1
TC-G-5	363	484	200	200	34.2%	1.33	1.1

The soft lubricants, SnAgCu, are mainly composed of Sn, Ag and Cu powders (5–45 μm in particle size and more than 99.92% purity), purchased from Nanjing XFNANO Materials Tech Co., Ltd. (Nanjing, China). The lubricants, CaF_2 (300–950 nm in particle size and more than 98.55% purity), are well mixed with the SnAgCu to construct nanolubricants, SnAgCu-CaF_2 (SC). Herein, SnAgCu is mainly composed of 90 wt.% Sn, 5 wt.% Cu and 5 wt.% Ag, and the SC consists of 75 wt.% SnAgCu and 25 wt.% CaF_2. The MSK-SFM-3 vibration mixer (Hefei Kejing Materials Technology Co., Ltd, Hefei, China) is used for homogeneous SC. Vibration power of 0.25 KW, a vibration frequency of 50 Hz, a mixing voltage of 220 V, a rated current of 1.99 A, and a mixing speed of approximately 1400 r/min are used in this study. The morphology of the SC mixture is characterized using the model No. Nova Nano-SEM 450 instrument (FEI Company, Hillsboro, OR, USA), and the FESEM (Field-Emission Scanning Electron Microscope, Nova NanoSEM 450, FEI (Thermo Fisher Scientific), Brno, Czech Republic) morphology of the SC is shown in Figure 1b. It can be seen from Figure 1b that the CaF_2 and SnAgCu are well mixed to acquire homogeneous SC powder.

The mixed SC lubricants are filled into the rectangular microgrids of the TC sample (TC-G) using hot-pressing sintering; subsequently, the micro/nanogrids (TCSC-G) are

successfully added into sliding plate surfaces. This preparation process can be described as follows: the microgrid samples and the SC lubricants are loaded into graphite molds, which are placed into an artificial intelligence box-type resistance furnace for hot infiltration heating. The infiltration temperature is chosen as 1100 °C, pressure is 0.16 MPa, initial temperature is 25 °C. The temperatures are raised to 1100 °C after 30 min, maintaining this temperature for 120 min, followed by subsequent cooling to 25 °C after 2.5 h. The TC-G samples, such as TC-G-1, TC-G-2, TC-G-3, TC-G-4 and TC-G-5, are well infiltrated using the SC lubricants under high-temperature atmosphere, which are correspondingly named as TCSC-G-1, TCSC-G-2, TCSC-G-3, TCSC-G-4 and TCSC-G-5. Before wear tests, the surfaces of as-prepared samples are mechanically polished using emery papers down to 1200 grits, leading to smooth surface textures with Sa (0.24 μm), Sq (0.22 μm), Sku (4.73) and Ssk (0.17), after ultrasonic cleaning five times.

2.2. Friction and Wear Measurements

To examine the tribological property of mechanical transmission sliding plates, dry sliding wear tests are carried out on the pure TC and TCSC-G samples. Figure 2 shows a typical schematic of the wear tests between TC samples and the Si_3N_4 balls. As shown in Figure 2, in accordance with ASTM Standard G99-95A (Standard Test Method for Wear Testing with a Pin-on-Disk Apparatus. ASTM International: West Conshohocken, PA, USA, 1995) [19,20], sliding wear tests on the different samples are conducted on a model No. MMX-1 tester, and a reciprocating line wear profile forms in the single surface. After five measurements at relative humidity of 55% and room temperature (25 °C), mean friction coefficients and wear rates are obtained. The surface roughness (Ra 1.6) of a Si_3N_4 ball (6 mm in diameter and 15 GPa in Vickers hardness) is examined. Under wear conditions of a 10 N load, 7 Hz frequency and almost 0.18 m/s, the friction coefficients are continuously recorded for 30 min using a computer control system. The ST400 surface profiler (Nanovea Inc., Irvine, CA, USA) is applied to measure the 3D profile of a wear scar, as shown in Figure 2. The 2D line profiles are continuously extracted from the 3D profiles to calculate the mean wear volume V of a wear scar after five times, and then the wear rate Q of the as-prepared sample is obtained. The specific calculation formulas are as follows [20]:

$$Q = \frac{V}{F \cdot S} \tag{1}$$

$$V = L \cdot A \tag{2}$$

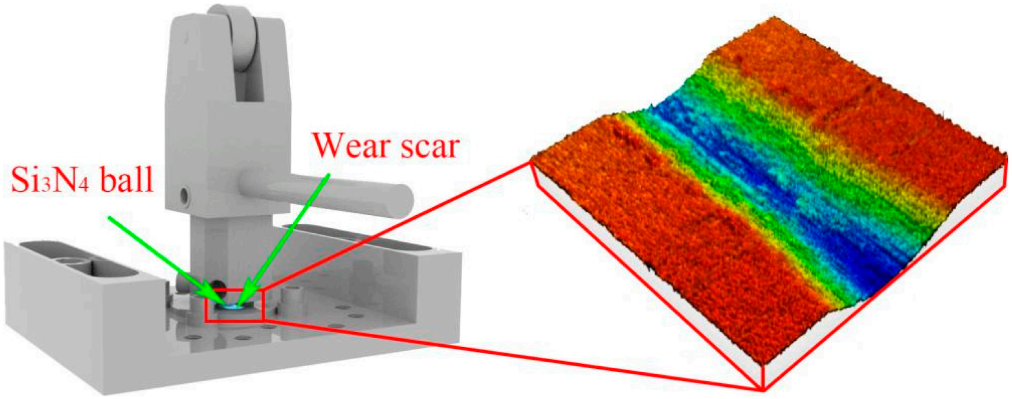


Figure 2. A friction schematic of the TC-base samples of mechanical transmission skateboard.

In these formulas, S is the total sliding distance (almost 327.6 m) for a wear test; F is the applied load (N); V is the wear amount (mm^3); L is the length (13 mm) of the sliding wear scar; A is the cross-sectional area of the wear scar (mm^2).

3. Test Results and Discussion

3.1. Hardness and Density of Proportional Micro/Nanogrid Structures

In accordance with ASTM Standard B962-08 and the Archimedes principle [20], the sample densities of TC and TCSC-G are tested across five measurements. The densities of the TC samples are mainly concentrated at 4.420~4.430 g/cm^3, with an average density of almost 4.426 g/cm^3. The densities of the TCSC-G are mainly concentrated in a range from 4.422 to 4.429 g/cm^3, and the mean densities (g/cm^3) are calculated as about 4.425 (TCSC-G-1), 4.425 (TCSC-G-2), 4.425 (TCSC-G-3), 4.424 (TCSC-G-4), and 4.424 (TCSC-G-5), respectively.

According to ASTM standard E92-82 [21], the digital Vickers hardness tester of model No. HVS-1000 is used to characterize the hardness for a dwell time of 10 s at 10 N. All tests are repeated five times, the hardness of TC is mainly 96.6~100.8 HV, and the average value is approximately 98.3 HV. The measured hardness values of the TCSC-G are mainly concentrated in 99.4~106.8 HV, and the mean hardness (HV) values are 103.1 ± 0.6 (TCSC-G-1), 103.0 ± 0.4 (TCSC-G-2), 103.1 ± 0.3 (TCSC-G-3), 103.5 ± 0.2 (TCSC-G-4), and 99.6 ± 0.5 (TCSC-G-5), respectively.

3.2. Analysis of Tribological Properties for Grid Structures

Table 2 shows the friction coefficients, wear rates and standard deviations (SDs) for the test samples. As can be seen from Table 2, if compared with those of TC samples, the TC-G samples acquire higher friction coefficients and a lower wear rate. If compared with those of the TC and TC-G, when the SC lubricants are filled into the micro-structures, the TCSC-G samples exhibit lower friction coefficients and wear rates, accompanied by smaller standard deviations. To visualize the tribological behaviors of the TC and TCSC-G, the mean friction coefficients and wear rates are indicated in Figure 3a,b. It can be seen from these figures and Table 2 that, if compared with pure TC, when the SC are filled into TC-G surfaces, the TCSC-G samples have lower friction coefficients and wear rates, coupled with smaller standard deviations. With an increase in structure lengths and widths, the mean friction coefficients and wear rates of the TCSC-G significantly decrease. With a sustained increase in lengths and widths, the mean friction coefficients and wear rates increase from TCSC-G-4 to TCSC-G-5. The TCSC-G-4 (length/width = 440:330) has the lowest friction coefficient of almost 0.23 and smallest wear rate of approximately 0.71×10^{-4} $mm^3N^{-1}m^{-1}$. Simultaneously, the friction coefficients are mainly distributed in the range of 0.22–0.24, while the wear rates are primarily concentrated at 0.69–0.73, resulting in the smallest SDs for friction coefficients (0.008) and wear rates (0.018).

To analyze the wear stability, the dynamic friction coefficients are shown in Figure 3c. As seen from Figure 3c, the sliding wear process of 1800 s can be divided into the running-in wear stage and stable stage. If compared with the TC samples, the TCSC-G samples have smaller fluctuations in friction coefficients. Compared with the tribological behaviors and SDs of the TCSC-G-1, TCSC-G-2, TCSC-G-3 and TCSC-G-5 samples, the TCSC-G-4 achieves lower and more stable friction coefficients. This is because the rectangular microstructure (length/width = 440:330) and nanolubricant SC produce the optimum synergistic function and lead to a significant improvement in the lubrication behaviors of the TCSC-G-4, thus making the tribological behavior of the TCSC-G-4 more stable and optimum.

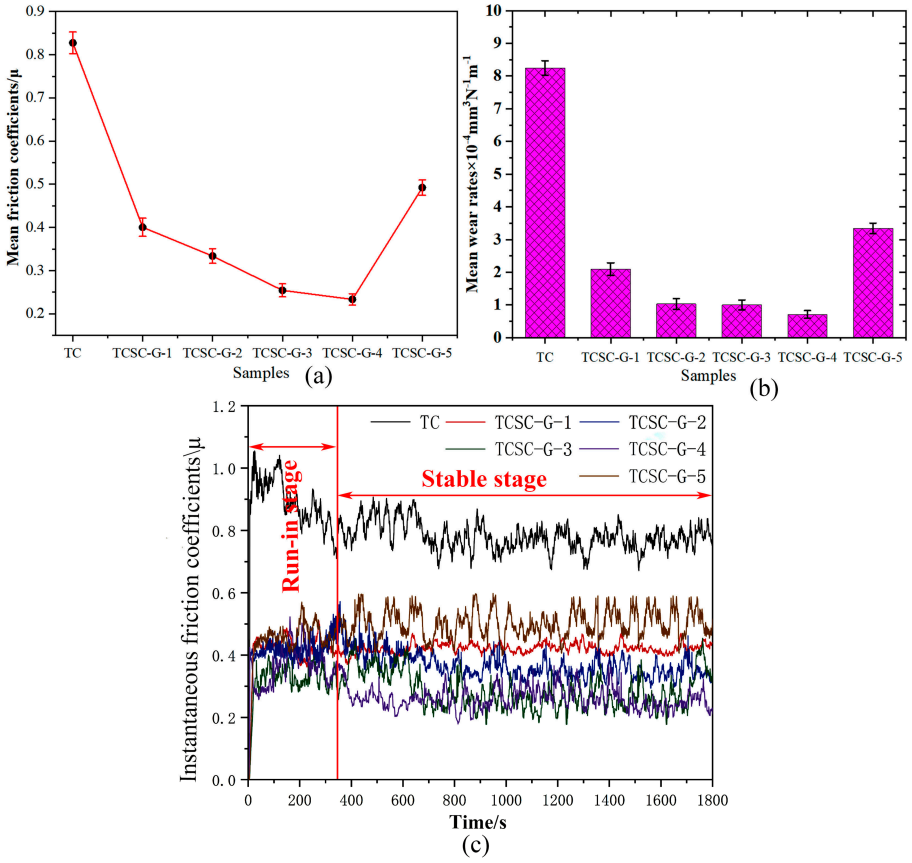


Figure 3. Tribological properties of the TC and TCSC-G: (**a**) average friction coefficients; (**b**) mean wear rates; (**c**) instantaneous friction coefficients.

Table 2. Friction coefficients, wear rates and standard deviations (SDs) for the test samples.

Sample Names	Friction Coefficients for Five Tests					Mean Values	Standard Deviation (SD)
TC	0.80	0.83	0.82	0.85	0.87	0.83	0.027
TCSC-G-1	0.45	0.43	0.40	0.35	0.37	0.40	0.041
TC-G-1	0.96	0.94	0.87	0.90	0.80	0.89	0.063
TCSC-G-2	0.35	0.36	0.32	0.31	0.30	0.33	0.026
TC-G-2	0.86	0.95	0.89	0.97	0.93	0.92	0.045
TCSC-G-3	0.29	0.27	0.24	0.25	0.22	0.25	0.027
TC-G-3	0.97	0.96	0.95	0.92	0.90	0.94	0.029
TCSC-G-4	0.23	0.22	0.23	0.22	0.24	0.23	0.008
TC-G-4	0.97	0.98	0.99	0.95	0.93	0.96	0.024
TCSC-G-5	0.48	0.42	0.53	0.47	0.53	0.49	0.046
TC-G-5	0.93	0.94	1.03	1.10	1.17	1.03	0.103
Sample Names	**Wear Rates ($\times 10^{-4}$ mm^{3}N^{-1}m^{-1}) for Five Tests**					**Mean Values**	**Standard Deviation (SD)**
TC	7.88	8.27	8.52	8.41	8.19	8.25	0.245
TCSC-G-1	1.81	2.04	2.25	2.20	2.21	2.10	0.182
TC-G-1	3.99	3.94	3.98	3.85	3.83	3.92	0.074
TCSC-G-2	0.93	1.05	0.97	1.12	1.06	1.03	0.076
TC-G-2	4.17	3.87	4.09	4.12	3.91	4.03	0.133
TCSC-G-3	0.94	1.07	0.97	0.94	1.09	1.00	0.073
TC-G-3	4.28	4.01	4.16	3.97	4.02	4.09	0.129
TCSC-G-4	0.69	0.69	0.72	0.73	0.71	0.71	0.018
TC-G-4	4.21	4.09	4.22	4.04	4.13	4.14	0.077
TCSC-G-5	3.13	3.37	3.41	3.74	3.04	3.34	0.274
TC-G-5	4.42	4.24	4.38	4.52	4.31	4.37	0.107

3.3. Analysis of Friction and Wear Mechanism

To explore the friction and wear properties of a TCSC-G, the FESEM morphologies of wear scars are shown in Figure 4. As shown in Figure 4a, the large-area spalling and a small amount of wear debris are accumulated on a wear scar of the TCSC-G-1, and peeling pits and sporadic island-shaped lubrication films are observed on the wear scar, accompanied by an abrasive wear scar. It results in a TCSC-G-1 wear rate of almost 2.10×10^{-4} $mm^3N^{-1}m^{-1}$ and almost 0.40 for the friction coefficient.

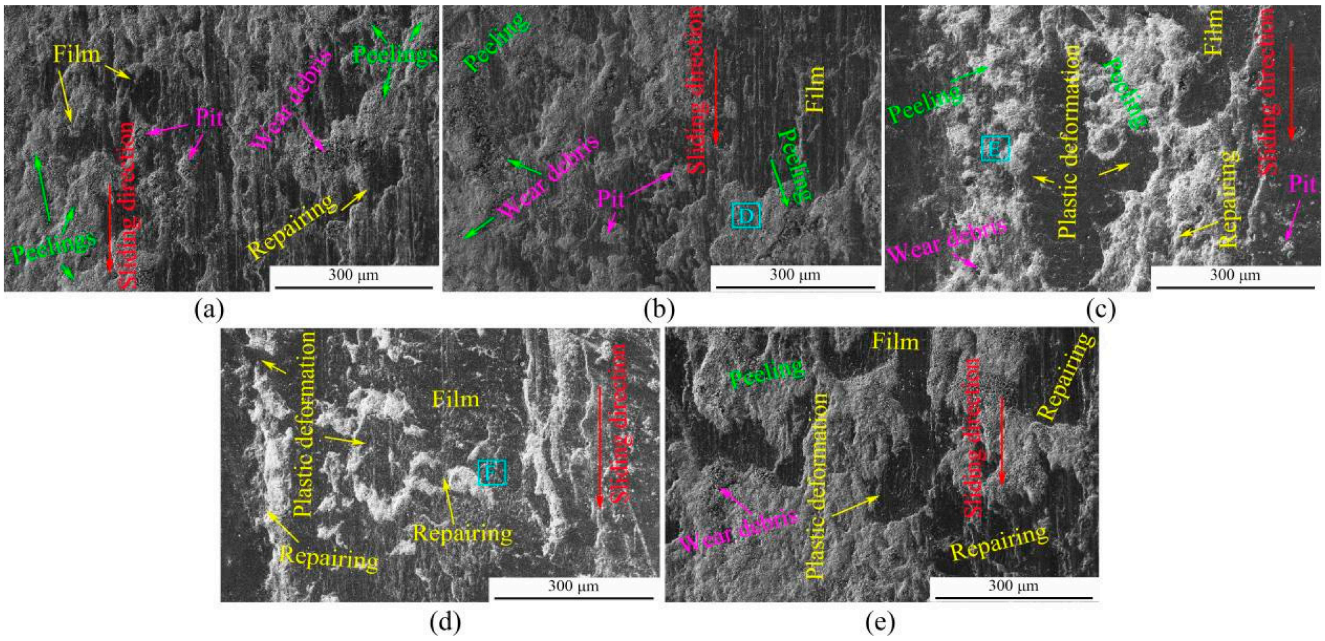


Figure 4. FESEM patterns showing the microcosmic morphologies of wear scars of the TCSC-G samples: (**a**) TCSC-G-1; (**b**) TCSC-G-2; (**c**) TCSC-G-3; (**d**) TCSC-G-4; (**e**) TCSC-G-5.

If compared with the TCSC-G-1, the wear scar of TCSC-G-2 has a smaller area of spalling, a small amount of wear debris and pits, and a large area of lubrication film, as shown in Figure 4b. The EDS results of the rectangular area D in Figure 4b are shown in Table 3. It can be seen from Table 3 that the main components of the spalling areas are the SC and TC-base material. It indicates that an increased area of the microgrid structure leads to the deformation of the edge structure, promotes SC migration toward a wear scar, and faces continuous spreading along the sliding direction, thus resulting in a large-area lubrication film for TCSC-G-2. It leads TCSC-G-2 to acquire a wear rate of about 1.03×10^{-4} $mm^3N^{-1}m^{-1}$ and a friction coefficient of almost 0.33, which are lower than those of the TCSC-G-1.

As can be seen from Figure 4c, there is a relatively complete lubrication film, a small amount of wear debris and micro-pits on the wear scar of the TCSC-G-3, accompanied by plastic deformation for repairing areas. The EDS results of the rectangular area E in Figure 4c are shown in Table 3. It can be seen from Table 3 that the lubrication film is mainly composed of SnAgCu and CaF_2. This is because the distribution area of the grid structure of the TCSC-G-3 increases, resulting in a decrease in bearing capacity. Under sliding wear force, large deformation occurs at the structure edges, generates a large amount of wear debris, enters the micro/nanogrid structure, and promotes a large amount of SC to migrate toward a wear scar, thus forming a lubrication film that protects the contact surface from damage. If compared with those of TCSC-G-2, the wear rate of TCSC-G-3 is about 1.0×10^{-4} $mm^3N^{-1}m^{-1}$, and the friction coefficient is about 0.25.

Table 3. Main element contents of the rectangles D, E and F on the wear scar in Figure 4.

The mass fraction of the rectangular area D in Figure 4b (wt.%)											
Ti	Al	F	Ca	Ni	O	C	B	V	Sn	Ag	Cu
17	12	10	9	-	17	8	-	-	14	5	8
The mass fraction of the rectangular area D in Figure 4c (wt.%)											
Ti	Al	F	Ca	Ni	O	C	B	V	Sn	Ag	Cu
11	13	9	12	-	14	8	-	-	20	5	8
The mass fraction of the rectangular area D in Figure 4d (wt.%)											
Ti	Al	F	Ca	Ni	O	C	B	V	Sn	Ag	Cu
8	9	8	12	-	21	7	-	-	22	4	9

The FESEM morphology of the wear scar of TCSC-G-4 is shown in Figure 4d. It can be seen from Figure 4d that large areas of the lubrication film, plastic deformation areas and the pit areas are found on the wear surface of TCSC-G-4. Table 3 shows the EDS results of the rectangular area F in Figure 4d. As shown in Table 3, the main components in the spalling areas are SnAgCu and CaF_2. This is because the distribution area of the microgrid structure of a TCSC-G-4 increases, leading to an increase in the SC in this structure. Under wear forces, the grid structure undergoes plastic deformation and promotes SC migration from the rectangular grid toward the wear scar. The SC lubricants continuously spread along the sliding direction, repair the surface micro-pits, and form a lubrication film that is distributed over a large area on a wear scar. During wear, spherical CaF_2 produces rolling wear, and SnAgCu undergoes good plastic deformation, thus forming mixed rolling–sliding wear. It reduces the sliding friction resistance and surface material loss and enhances the friction-reducing and wear-resistant abilities of the lubrication film. Therefore, under the synergistic lubrication of grid structure and the SC, the TCSC-G-4 achieves an optimum tribological property, along with an average wear rate of approximately 0.71×10^{-4} $mm^3N^{-1}m^{-1}$ and a friction coefficient of about 0.23.

FESEM morphologies of the wear scars of the TCSC-G-5 are shown in Figure 4e. As indicated in Figure 4e, there are large-area spalling regions and a large amount of wear debris on the wear scar of TCSC-G-5, accompanied by sporadically dendritic lubrication films. It is because the distribution area of microgrid structures in the wear scar increases, which leads to a decrease in bearing ability and makes it difficult to resist the surface damage, thus forming large-area spalling and a large amount of wear debris. Simultaneously, a low bearing ability cannot easily support lubrication film formation and results in a sporadically dendritic lubrication film. Therefore, if compared with those of TCSC-G-4, the TCSC-G-5 has reduced lubrication, with a wear rate of approximately 3.34×10^{-4} mm^3 N^{-1} m^{-1} and a friction coefficient of about 0.49.

To further analyze the sliding wear properties of the test samples, the morphology is scanned to characterize a wear scar. The magnified FESEM morphology of the TCSC-G-2 wear surface is shown in Figure 5a. It is not difficult to find a small amount of wear debris and microcosmic pits, slight spalling, a small area of lubrication film and the repair areas in Figure 5a. Due to the surface damage caused by wear forces, it results in micro-spalling and pit formation; subsequently, the spalling debris aggravates the surface damage. The grid structure cannot easily provide sufficient SC for the wear scar; it is difficult to repair the friction damage, and the spalling damage is greater than the surface repair of the lubricants, leading to a small amount of wear debris and pits, slight spalling, a small area of lubrication film and repairing areas. Figure 5b shows the 3D height cloud distribution of the scanning area (4000 μm × 4000 μm) on the wear scar, and the corresponding height parameters are shown in Table 4. A depth cloud distribution of the scanning area of a TCSC-G-2 wear

scar is shown in Figure 5c. The 2D line profile of the height distribution along the straight line AA of Figure 5c is shown in Figure 5d. The main height parameters of Figure 5d are shown in Figure 5e, where the main height of 50.000–183.334 μm accounts for about 45%; this proves the uneven wear surface of TCSC-G-2, meaning the friction-reducing and wear-resistant properties of the TCSC-G-2 are not ideal.

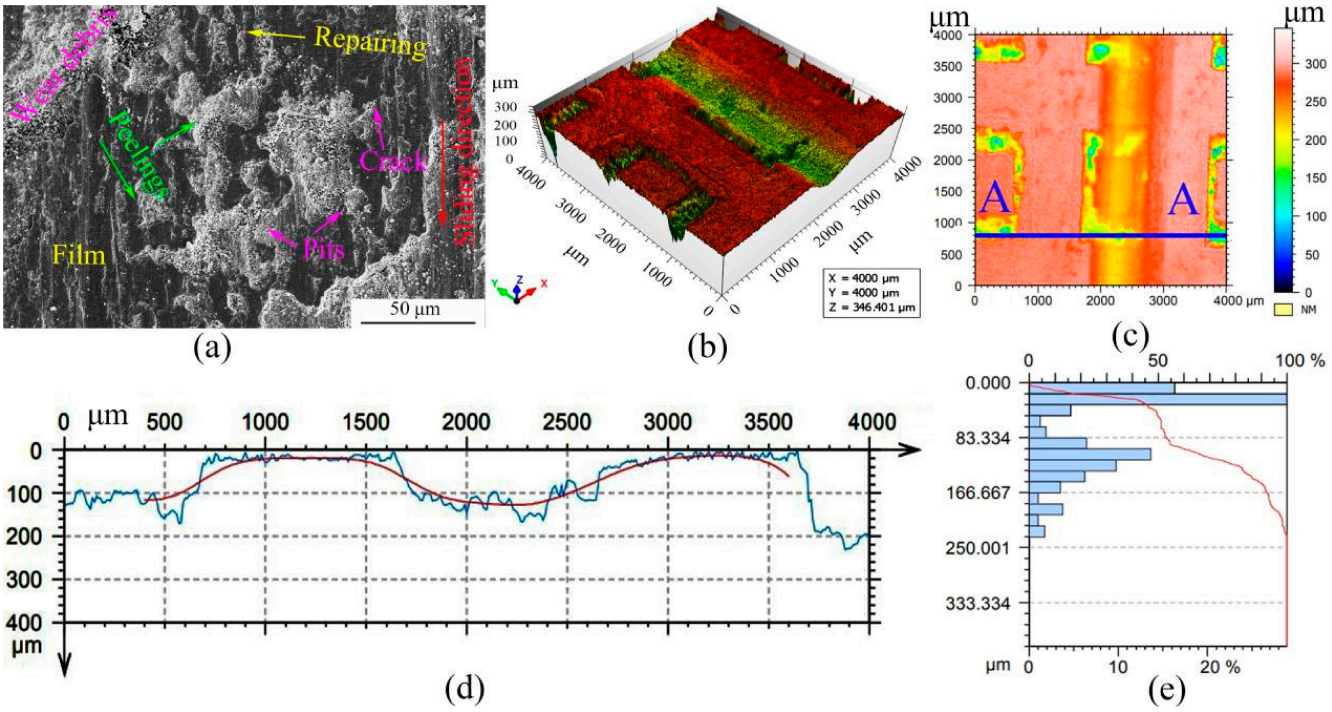


Figure 5. Scanning morphologies and characteristic curves of the wear scars of a TCSC-G-2: (**a**) FESEM morphology; (**b**) 3D height distribution; (**c**) cloud distribution of the wear scar depth; (**d**) 2D height distribution of the line AA in (**c**); (**e**) statistical chart of main height parameters of (**d**).

Table 4. Surface heights after the tests for the TCSC-G-2 sample.

Height Parameters	Values	Height Parameters	Values
Root Mean Square Height (Sq)/μm	37.281	Maximum Pit Height (Sv)/μm	2.70210×10^{-2}
Skewness (Ssk)	−1.839	Maximum Height (Sz)/μm	3.46401×10^{-2}
Kurtosis (Sku)	6.739	Arithmetic Mean Height (Sa)/μm	2.8752×10^{-1}
Maximum Peak Height (Sp)/μm	76.192	Inverse Areal Material Ratio (Smr)/%	6.219×10^{-4}

The magnified FESEM morphology of the TCSC-G-3 wear scar is shown in Figure 6a. It can be seen from Figure 6a that there are large areas of lubrication film and plastic deformation regions on the wear scar, and small areas of the repair regions and a small amount of wear debris can be found. It is because during wear, the SC precipitate from the grid structure to the wear scar and form a lubrication film that distributes over a large area. Subsequently, the lubrication film undergoes deformation and then slowly flows to the wear-damaged regions to repair the wear scars. Due to insufficient SC supplementation, only a small area of the wear scar can be repaired. This results in TCSC-G-3 having lower friction resistance and material loss, if compared with the TCSC-G-2, along with a wear rate of approximately 1.0×10^{-4} $mm^3N^{-1}m^{-1}$ and a friction coefficient of about 0.25.

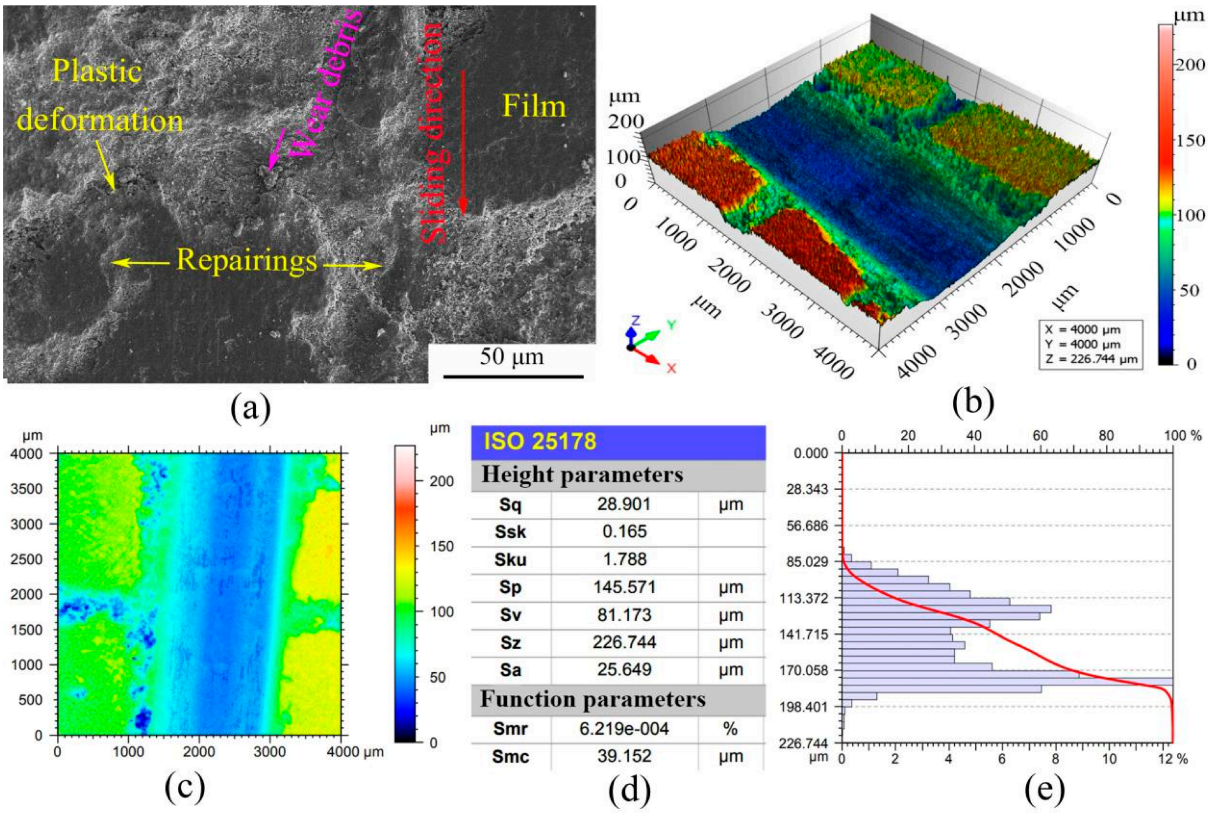


Figure 6. Scanning morphologies and characteristic curves of the wear scars of the TCSC-G-3: (**a**) FESEM morphology of wear scar; (**b**) 3D height distributions; (**c**) cloud distribution of the wear scar depth; (**d**) 3D heights of wear scar; (**e**) bar statistical distributions of main height parameters of (**b**).

The 3D morphology of the scanning area (4000 μm × 4000 μm) of a wear scar is shown in Figure 6b. The 3D height cloud distribution of the scanning area and its height parameters are shown in Figure 6c,d. Figure 6e presents the statistical results and columnar distribution of the main height parameters in Figure 6b. As shown in Figure 6e, the micro-heights of 79.360–136.046 μm account for 47% of the total height of the TCSC-G-3 wear scar. If compared with the statistical result (45%) of TCSC-G-2, the statistical proportion (47%) of TCSC-G-3 is larger, indicating that the wear scar is relatively flat. It is because, if compared with those of the TCSC-G-2, the grid distribution area of the TCSC-G-3 increases, and then the stored SC are increased. During wear, the SC fill the damaged areas and repair the uneven wear scar. Due to insufficient SC precipitation, the repairing ability of the wear scar is insufficient and results in the TCSC-G-3 having a relatively flat wear scar. It is beneficial for reducing frictional resistance and material loss and leads to better friction-reducing and wear-resistant properties of the TCSC-G-3, if compared with that of the TCSC-G-2.

To observe the wear scar of TCSC-G-4, magnified FESEM morphology is shown in Figure 7a. As can be seen from Figure 7a, a relatively complete lubrication film, the large plastic deformation regions and large-area repairing regions are distributed on the wear scar, accompanied by a small amount of wear debris and small pits. This is because the SC of a TCSC-G-4 appear on the wear scar, provide sufficient SC for the ideal self-repairing of surface damage, which balances surface damage and self-repair, and promotes the formation of a complete lubrication film. This film is well distributed between the friction pairs, significantly reducing the surface material damage, thus leading to a small amount of wear debris and small pits of the wear scar.

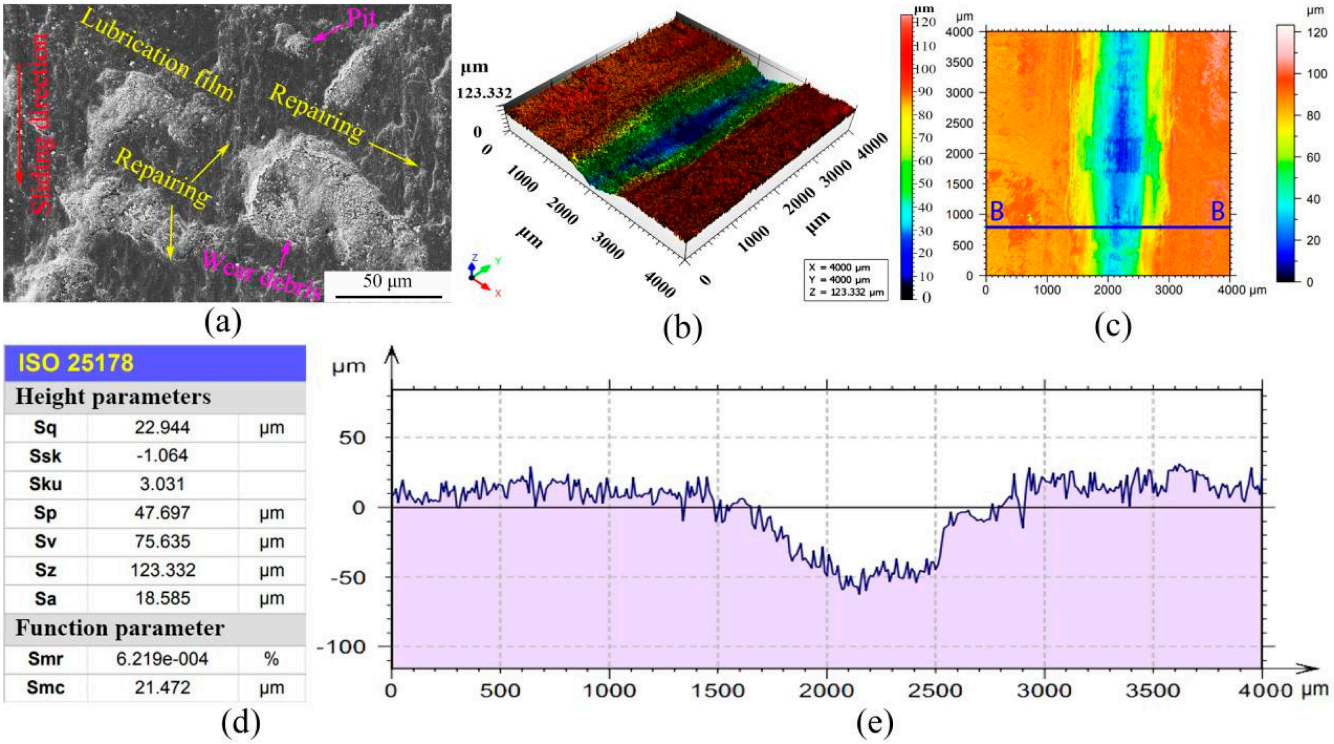


Figure 7. Scanning morphologies and characteristic curves of the wear scar of TCSC-G-4: (**a**) FESEM morphology of wear scar; (**b**) cloud distribution of 3D heights; (**c**) cloud distribution of wear scar depth; (**d**) 3D height parameters; (**e**) 2D height distribution along the line BB of (**c**).

Figure 7b shows the 3D morphology of the scanning area (4000 μm × 4000 μm) of a wear scar. Figure 7c shows the 3D micro-height cloud distribution. Figure 7d presents the 3D height parameters of Figure 7b. Figure 7e shows the 2D height profile along the line BB in Figure 7c. As shown in Figure 7b–e, if compared with the TCSC-G-3, the TCSC-G-4 wear scar has smaller Root Mean Square Height (Sq: 22.944 μm) and arithmetic mean height (Sa: 18.585 μm). This indicates that the wear scar of TCSC-G-4 is effectively repaired and forms a relatively smooth wear scar. It is mainly attributed to the plastic flow of SC on the wear scar, which effectively fills the damaged areas and repairs the wear scar, thus resulting in a smooth wear scar for TCSC-G-4. It is conducive to reductions in friction coefficients and wear rates.

The FESEM morphology of the TCSC-G-4 is shown in Figure 8a. In Figure 8a, the wear debris is mostly fine spherical particles and small paper-like structures. This indicates that the wear scar of TCSC-G-4 is subject to microdamage and forms flaky wear debris, which is continuously refined to form the fine spherical particle under frictional force. Together with the SC, these particles are filled into the damage areas, forming large-area repair areas and promoting lubrication film formation on the wear scars. The C element in Figure 8b is mainly derived from the conductive adhesive, that is, the carrier for the wear debris tests. Figure 8c–g show the distribution states of Ca, F, Sn, Ag and Cu elements. The presence of Ca, F, Sn, Ag and Cu elements indicates that CaF_2 and SnAgCu appear in the wear debris. Figure 8h,i show the distributions of Ti and Al elements, which are mainly derived from the TC-base material. These results show that during the friction and wear process, the microdamage occurs on a wear scar and forms paper-like and spherical wear debris. The wear debris and SC repair the damaged areas, and the excess wear debris detaches from a wear scar at centrifugal forces, thereby resulting in material loss of the wear scar.

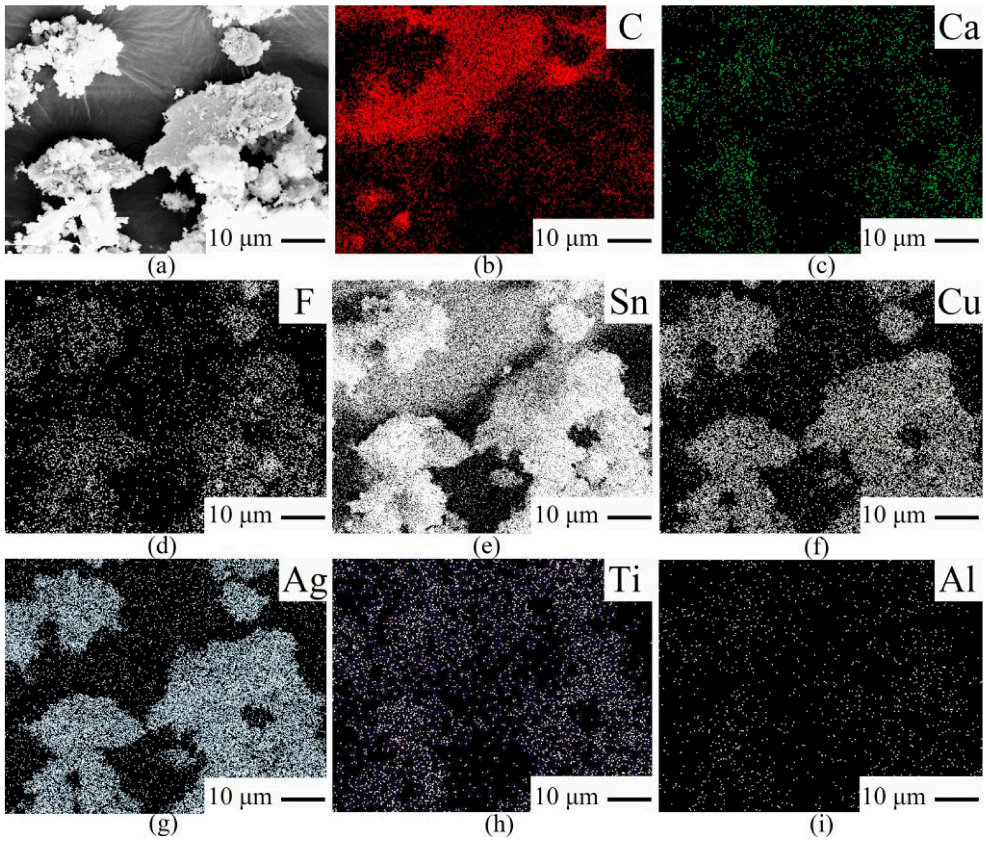


Figure 8. FESEM morphologies (**a**) and main element distributions (**b**–**i**) of the wear debris of the TCSC-G-4.

In order to analyze the effect of the wear scar subsurface on tribological properties, the wear scar cross-sections of TCSC-G-3 and TCSC-G-4 are studied, and the results are shown in Figure 9. Figure 9a shows the layered cross-section structures of TCSC-G-3. During wear, the SC lubricants precipitate to enrich on the wear scar, forming a layer of the lubrication film, and then the micro-deformed layer is formed to support this lubrication film to achieve the friction-reducing and wear-resistant behaviors. Figure 9b shows the FESEM morphology of the wear scar cross-section of the TCSC-G-4. As can be seen from Figure 9b, there is an obvious layer structure that is composed of the lubrication film, enhancement layer and the micro-deformed layer. It is because the increased sizes of the microgrid structures lead to greater SC storage and a decrease in surface bearing ability, prompting large plastic deformation under friction force, which causes the SC to form a lubrication film. At the same time, the enhancement layer formation is attributed to the continuous grain refinement on the wear scar subsurface, and the micro-deformed layer benefits from grain deformation. If compared with the TCSC-G-3, the lubrication layer forms on a wear scar of the TCSC-G-4, which is more complete and larger. During wear, the enhancement layer provides a stable support for the friction-reducing and wear-resistant behaviors of the lubrication film, and then the micro-deformed layer realizes the transition from a lubrication film to the matrix layer, thus enhancing the bonding forces between the two. It is conducive to improving the friction-reducing and wear-resistant properties of the TCSC-G-4.

Figure 10 shows the FESEM morphology and main element distribution of a TCSC-G-4 wear scar. As shown in Figure 10a,b, massive SC are enriched on a wear scar, forming a multilayer lubrication film on the wear scar micro-area. This is because in the friction and wear process, the lubricants precipitate to spread layer by layer on the wear scar, thus leading to the formation of a layer-structured lubrication film. Under the repeated

action of friction forces, the lubrication film undergoes micro-spalling, resulting in the layer structures of the wear scar. Figure 10b shows the superimposed distribution morphology of the main elements. Figure 10c,d show the distribution of Ti and Al elements; this indicates the matrix exposure on the wear scar for spalling. The elements, Sn, Ag and Cu, appear in Figure 10e–g, confirming that SnAgCu appears in the lubrication film. The elements in Figure 10h,i are Ca and F, ensuring that spherical CaF_2 appears on a wear scar. The aforementioned discussions show that the SC combine with wear debris to form a layer of the lubrication film. The wear force promotes the plastic flow of the lubrication film to fill the damaged areas, enhance the repairing ability of wear scar, and then obtain a relatively smooth morphology, thus improving the friction-reducing and wear-resistant properties of the TCSC-G-4.

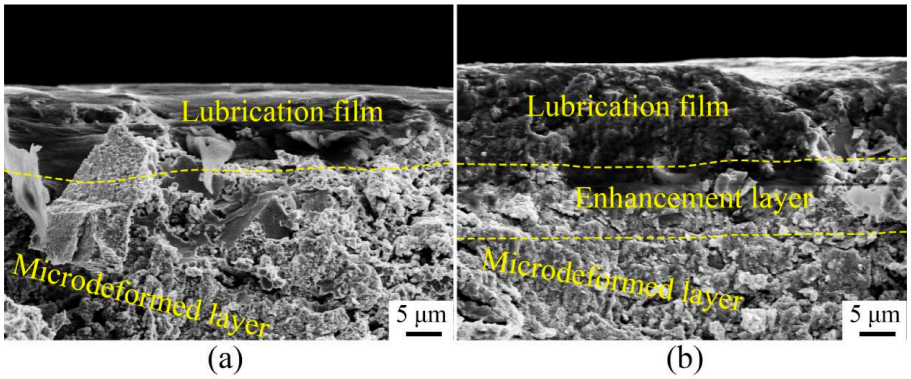


Figure 9. FESEM morphologies of wear scar cross-sections of the as-prepared sample: (**a**) TCSC-G-3; (**b**) TCSC-G-4.

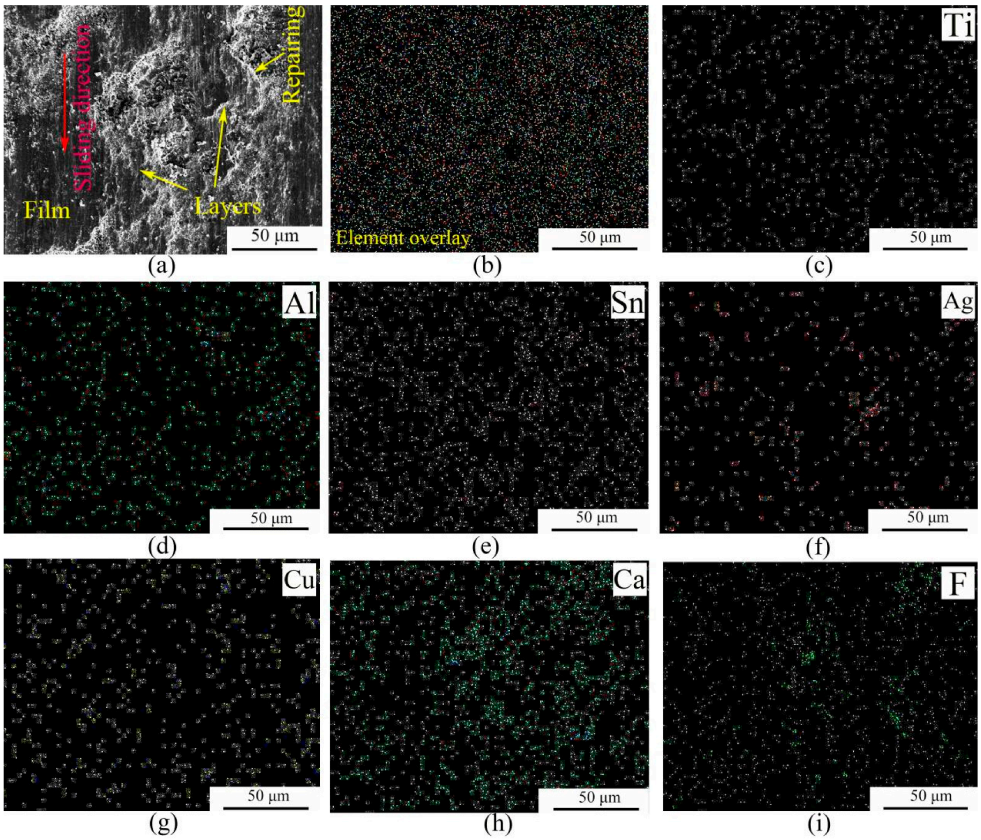


Figure 10. Microscopic morphologies (**a**) and main element distributions (**b**–**i**) of the wear scars of a TCSC-G-4.

To observe the multilayer structure of a TCSC-G-4 lubrication film, magnified FESEM morphology is shown in Figure 11a. It can be seen from FESEM morphologies of the numbered positions 1–4 in Figure 11a that a four-layer structured film forms on a wear scar. EDS analysis is carried out on each layer structure of the lubrication film. The results show that the mass fractions (wt.%) of the main elements in the rectangle regions A, B, C and D are (21.37–24.35)-Sn, (7.12–8.95)-Cu, (5.97–7.52) -Ag, (11.34–14.21)-Ca, (9.77–11.73)-F, (12.15–14.27)-O, (0.51–0.92)-C, (13.29–16.72)-Ti, (8.91–10.17)-Al. It confirms that the multilayer lubrication film contains a large amount of SnAgCu and CaF_2.

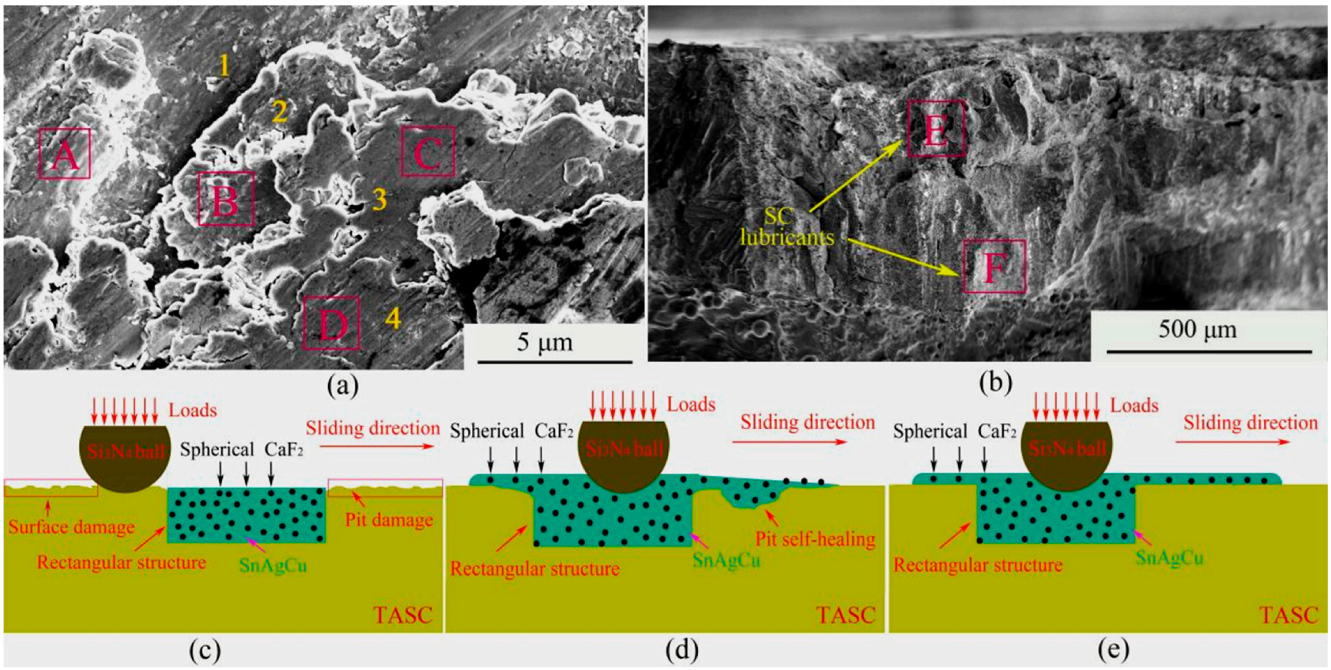


Figure 11. FESEM morphologies of surface (**a**) and cross-section (**b**) of the wear scars; formation of lubrication film and lubrication mechanism (**c**–**e**) of the TCSC-G-4.

Figure 11b shows the FESEM morphology of the wear scar cross-section of TCSC-G-4. An EDS analysis is performed on the rectangular regions E and F in Figure 11b, and the results indicate that the mass fractions (wt.%) of the main elements in region E are 21.42-Sn, 8.25-Cu, 6.31-Ag, 13.12-Ca, 10.27-F, 13.19-O, 0.42-C, 16.71-Ti, and 10.01-Al; the mass fractions (wt.%) of the main elements in region F are 21.03-Sn, 7.16-Cu, 7.44-Ag, 13.01-Ca, 11.23-F, 12.36-O, 0.91-C, 16.12-Ti, and 9.23-Al. This indicates that the wear scar cross-section in Figure 11b contains a large amount of SC.

Figure 11c–e show the formation process and lubrication mechanism of the lubrication film of TCSC-G-4. It can be seen from the figures that during wear, the TC surface is subject to wear damage, which results in micro-spalling and small pits, as shown in Figure 11c. Simultaneously, a large amount of SC precipitate from these grid structures toward the wear scars, which ensures the lubricant demand of the friction surface. Under the effective action of wear forces, the plastic flowing occurs and continuously spreads layer by layer to fill into the micro-damaged spalling areas and pits, as shown in Figure 11d. During wear, the SC are enriched on a wear scar, forming a layer-structured lubrication film on the repair region, as shown in Figure 11e.

During wear, normal loads and friction forces cause good migration of SC from the grid structure toward a wear scar. Subsequently, plastic deformation occurs to spread on a wear scar and results in a homogeneous lubrication film containing the SC during sliding wear. The SnAgCu in the film has a low shear strength and high viscosity fluid-like

lubrication characteristics [22], undergoes good deformation, and reduces wear resistance and material loss. CaF_2 has high hardness and spherical-structured characteristics [23,24]. The CaF_2 particles are coated in SnAgCu, producing rolling wear and enhancing the plastic deformation of SnAgCu. Meanwhile, SnAgCu is coated on the surface of CaF_2 particles, enhancing their rolling wear and significantly reducing the sliding friction resistance and surface material loss. A good deal of CaF_2 particles are enriched in the lubrication films, improving the bearing abilities and resisting the wear scar damage, thus reducing the micro-damage of the wear scar. During wear, the lubrication film exists between the frictional pairs and forms the new-style wear contact interface. In this film, the CaF_2 undergoes good rolling during wear and increases the plastic deformation of SnAgCu. This deformation is conducive to enhancing spherical rolling of CaF_2, and the result in effective collaboration lubrication of SC. It improves the lubrication behavior of the wear pair and leads to optimum tribological properties for TCSC-G-4.

4. Conclusions

To improve the friction and wear properties of a mechanical transmission sliding plate, this study focuses on the tribological behavior of rectangular micro/nanogrid structures containing SC, and we offer the following conclusions:

(1) If compared with TCSC-G-1, TCSC-G-2, TCSC-G-3 and TCSC-G-5, TCSC-G-4 (length/width = 440:330) has the optimum lubrication properties and acquires the lowest friction coefficient of about 0.23 and smallest wear rate of approximately 0.71×10^{-4} mm^3 N^{-1} m^{-1}.

(2) Micro-deformation of the grid structure causes the precipitation of massive SC in the grid structures toward the wear scar and spreads to form the lubrication film. This helps to resist wear damage and enables TCSC-G-4 to achieve the optimum tribological properties.

(3) During wear, the sliding wear mechanism is transformed into a mixture mechanism, which is dominated by rolling, sliding and rolling–sliding. It reduces the frictional resistance and material loss for an optimum tribological property of the TCSC-G-4.

(4) During wear, the SC and wear debris synergistically produce plastic flow, fill into the damage areas, acquire good repair of the wear scar, and enhance the contact stability, thus enabling TCSC-G-4 to achieve an optimum and stable tribological property.

(5) Massive SC are enriched in the lubrication film to improve the plastic deformation and bearing abilities. CaF_2 rolling helps with SnAgCu deformation and enhances the CaF_2 rolling in turn, thus leading to TCSC-G-4 having an optimum and stable tribological property.

Author Contributions: Conceptualization, K.Y.; methodology, J.T. and K.Y.; formal analysis, K.Y., J.T. and Y.W.; investigation, Y.W. and K.Y.; resources, K.Y., Y.W. and J.T.; data curation, J.T. and Y.W.; writing—original draft preparation, Y.W. and J.T.; writing—review and editing, K.Y. and Y.W.; visualization, K.Y. and Y.W.; supervision, K.Y. and Y.W.; project administration, Y.W. and J.T.; funding acquisition, K.Y. All authors have read and agreed to the published version of the manuscript.

Funding: This study was mainly supported by the Natural Science Foundation of Henan Province (262300420053 and 262300420417), Project for the Science and Technology Plan of Henan Province (252102221038).

Data Availability Statement: The original contributions presented in the study are included in the article; further inquiries can be directed to the corresponding authors.

Acknowledgments: This study was mainly supported by the Promotion Projects of Anyang City (2025C01GX024), the Initial Scientific Research Fund of PhD in the Anyang Institute of Technology (BSJ2025031), Initial Scientific Research Fund of Postdoctor in the Anyang Institute of Technology

(BHJ2025010), the Henan postdoctoral Science Foundation (HN2025153), the Key Scientic Research Project Plan of Higher Education Institutions of Henan Province (25B460009); Henan Mechanical Engineering Master Teacher Studio (ZLG202320); and Zhengzhou City Mechanical and Electronic Engineering Master Teacher Studio (ZZLG202401). The authors are also appreciative of Nanjing XFNANO Materials Tech Co., Ltd. for their kind assistance.

Conflicts of Interest: The authors declare no conflicts of interest.

References

1. Zhao, B.; Zhang, S.; Li, J.F.; Wang, P. Friction characteristics of sliding guideway material considering original surface functional parameters under hydrodynamic lubrication. *Proc. Inst. Mech. Eng. Part J.-J. Eng. Tribol.* **2017**, *231*, 813–825. [CrossRef]
2. Franco, O.; Beudaert, X.; Erkorkmaz, K.; Munoa, J. Influence of guideway friction on the cutting point receptance in machine tools. *Cirp Ann.-Manuf. Technol.* **2022**, *71*, 361–364. [CrossRef]
3. He, Y.Y.; Fu, Y.H.; Wang, H.; Yang, J. Enhancing anti-stick-slip performance by laser surface texturing on sliding guideway surface. *J. Manuf. Process.* **2022**, *75*, 1089–1099. [CrossRef]
4. Bao, H.; Hao, M.J.; Du, Y.C.; Chen, Y.Z. Optimal Design of Multilevel Composite Lubrication Structures on Sliding Guide Rail Surfaces. *Coatings* **2024**, *14*, 1286. [CrossRef]
5. Ouyang, J.H.; Li, Y.F.; Zhang, Y.Z.; Wang, Y.M.; Wang, Y.J. High-Temperature Solid Lubricants and Self-Lubricating Composites: A Critical Review. *Lubricants* **2022**, *10*, 177. [CrossRef]
6. Liu, S.B.; Gong, H.Y.; Qian, Y.; Zhao, J.B.; Ye, H.C.; Zhang, Z.Q. The friction and wear performance of polytetrafluoroethylene coating reinforced with modified graphene. *Mater. Today Commun.* **2022**, *31*, 103448. [CrossRef]
7. Chen, K.Y.; Yang, X.F.; Lv, G.J.; Zhang, Y.F.; Yang, H.; Gao, Y.L. Research progress of surface modification and solid-liquid lubrication synergistic friction reduction and wear resistance. *Int. J. Adv. Manuf. Technol.* **2022**, *122*, 1115–1141. [CrossRef]
8. Shan, Z.Q.; Jia, X.H.; Li, S.; Li, Y.; Yang, J.; Fan, H.Z.; Song, H.J. Self-lubricating and wear-resistant epoxy resin coatings based on the "soft-hard" synergistic mechanism for rapid self-healing under photo-thermal conditions. *Chem. Eng. J.* **2024**, *481*, 148664. [CrossRef]
9. Shen, G.; Zhang, J.F.; Kang, C.W.; Fang, F.Z. Study on surface texture patterns for improving tribological performance of bioimplants. *Surf. Coat. Technol.* **2021**, *422*, 127567. [CrossRef]
10. Torres, H.; Ripoll, M.R.; Prakash, B. Tribological behaviour of self-lubricating materials at high temperatures. *Int. Mater. Rev.* **2018**, *63*, 309–340. [CrossRef]
11. John, M.; Menezes, P.L. Self-Lubricating Materials for Extreme Condition Applications. *Materials* **2021**, *14*, 5588. [CrossRef] [PubMed]
12. Zhou, Z.R. Tribology in China. *Friction* **2025**, *13*, 9440994. [CrossRef]
13. MacLucas, T.; Grützmacher, P.G.; Leonhard-Trautmann, P.; Suarez, S.; Gachot, C.; Mücklich, F. Combining Carbon Nanoparticle Coatings and Laser Surface Texturing for Enhanced Lubricity Under High Loads. *Tribol. Lett.* **2024**, *72*, 38. [CrossRef]
14. Tankal, K.; Güney, B.; Erden, M.A. A comparative study of thermal sprayed Al_2O_3-TiO_2 coatings on PM AISI 316L. *Eng. Sci. Technol. Int. J.* **2024**, *60*, 101895. [CrossRef]
15. Ma, L.S.; Fu, S.; Li, J.; Lu, Y.N.; Li, X.C.; Qi, J.H.; Chen, J.W. Combining laser biomimetic surface microtextured and PTFE solid lubricant for improved friction property of Ti6Al4V. *Sci. Rep.* **2025**, *15*, 10457. [CrossRef] [PubMed]
16. Liu, Y.; Zhang, H.; Dai, S.J.; Dong, G.N. Designing a bioinspired scaly textured surface for improving the tribological behaviors of starved lubrication. *Tribol. Int.* **2022**, *173*, 107594. [CrossRef]
17. Chen, S.Q.; Dai, Q.W.; Yang, X.L.; Liu, J.J.; Huang, W.; Wang, X.L. Bioinspired Functional Structures for Lubricant Control at Surfaces and Interfaces: Wedged-Groove with Oriented Capillary Patterns. *ACS Appl. Mater. Interfaces* **2022**, *14*, 42635–42644. [CrossRef] [PubMed]
18. Miao, C.; Yin, X.; Yang, K.; Zhang, C.; Meng, Y. Successful Fabrication of Hydrophobic Surfaces of Microstructures Cooperating with Solid–Liquid Nanomaterials on the CuZnPb Alloy Substrate. *Langmuir* **2023**, *39*, 12550–12562. [CrossRef] [PubMed]
19. Chen, Q.; Zhang, J.J.; Huang, A.G.; Wei, P.Y. Study on Wear Resistance of Ti-6Al-4V Alloy Composite Coating Prepared by Laser Alloying. *Appl. Sci.* **2021**, *11*, 446. [CrossRef]
20. Yang, K.; Ma, H.; Liu, X.; Zhang, Y.; He, Q. Multiwalled carbon nanotubes enhanced the friction layer evolution and self-lubricating property of TiAl-10 wt% Ag-1 wt% MWCNTs sample. *RSC Adv.* **2017**, *7*, 40592–40599. [CrossRef]
21. *ASTM E92-82*; Standard Test Method for Vickers Hardness of Metallic Materials. ASTM International: West Conshohocken, PA, USA, 2003.
22. Xue, Y.W.; Wu, C.H.; Shi, X.L.; Huang, Q.P.; Ibrahim, A.M.M. Effects of groove-textured surfaces filled with Sn-Ag-Cu and MXene-Ti_3C_2 composite lubricants on tribological properties of CSS-42L bearing steel. *Friction* **2022**, *10*, 1091–1113. [CrossRef]

23. Sadrabadi, P.; Durst, K.; Göken, M. Study on the indentation size effect in CaF_2: Dislocation structure and hardness. *ACTA Mater.* **2009**, *57*, 1281–1289. [CrossRef]
24. Thangudu, S.; Natarajan, A.; Mehta, S.; Devarakonda, K.P.; Massoud, T.F.; Paulmurugan, R. Scalable Synthesis of Calcium Fluoride Nanoparticles as a Novel Ultrasound Contrast Agent for Imaging Tumor Targeted Delivery of Therapeutics. *Chem. Biomed. Imaging* **2026**, *4*, 1202–1213. [CrossRef] [PubMed]

Disclaimer/Publisher's Note: The statements, opinions and data contained in all publications are solely those of the individual author(s) and contributor(s) and not of MDPI and/or the editor(s). MDPI and/or the editor(s) disclaim responsibility for any injury to people or property resulting from any ideas, methods, instructions or products referred to in the content.